Pergamon

Int. J. Solids Structures Vol. 35, Nos 28–29, pp. 3815–3830, 1998

0020–7683/98 $19.00 + .00

PII: S0020–7683(97)00220–5

INTEGRATED STRUCTURAL/CONTROL OPTIMIZATION OF LARGE ADAPTIVE/SMART STRUCTURES

H. ADELI*
Department of Civil and Environmental Engineering and Geodetic Science, The Ohio State University, 470 Hitchcock Hall, 2070 Neil Avenue, Columbus, OH 43210-1275, U.S.A.

and

A. SALEH
Analysts International Corporation, 471 E, Broad Street, Columbus, OH 43215, U.S.A.

(*Received* 14 *March* 1997; *in revised form* 8 *July* 1997)

Abstract—The authors recently presented a general computational model for active control of large structures subjected to dynamic loadings such as impact, earthquake, or wind loadings through integration of four different technologies: control theory, optimization theory, sensor/actuator technology, and high-performance computing. In this extension of the research, the computational model is generalized by simultaneous minimization of the weight of the structure and the required level of control forces. The solution of the integrated structural/control optimization problem for large structures requires high-performance computing resources. A new parallel-vector algorithm has been developed for computation of the closed loop eigenvalue and damping factor sensitivities. The computational model and parallel vector algorithms have been applied to both steel bridge and multistorey space frame structures subjected to various types of dynamic loadings such as impulsive traffic, wind, and earthquake loadings. It is concluded that through adroit use of controllers, the weight of the minimum weight structure can be reduced substantially. This research provides the foundation for design and construction of a new generation of high-technology adaptive/smart structures. © 1998 Elsevier Science Ltd. All rights reserved.

1. INTRODUCTION

The use of active control systems is a promising approach to minimize the structural damage to bridges, buildings, and other structures due to dynamic loadings such as earthquake and wind vibrations (Liu *et al.*, 1991, Housner *et al.*, 1996 and Kobori, 1996). Successful creation of such adaptive or smart structures requires ingenious integration of three different technologies: control, optimization, and sensor/actuator technology. The need for integration of control and optimization theories arises because of the desire to minimize both the required level of control forces and the weight of the structure. The formulation of such an integrated structural/control optimization problem is complex. Its solution for large structures with a few hundred members and more requires high-performance computing resources in terms of both memory and CPU. Thus, there is a need to develop efficient concurrent algorithms utilizing the unique architecture of multiprocessor supercomputers (Adeli, 1992a,b and Adeli and Kamal, 1993).

In a recent article, the authors presented a general computational model for active control of large structures subjected to dynamic loading such as impact, earthquake, or wind loadings (Adeli and Saleh, 1997). Parallel algorithms were developed for solution of the complex eigenvalue problem encountered in both open loop (without controllers) and closed loop (with controllers) systems (Saleh and Adeli, 1996), the resulting Riccati equation (Saleh and Adeli, 1997), and computation of the response of the structure. We applied the model to various kinds of bridge and multistorey building structures and investigated various arrangements for placement of the controllers. For a given structure the response

* Author to whom correspondence should be addressed.

was minimized employing appropriately placed controllers. No attempt was made to optimize the weight of the structure.

When the response of a structure (displacement and stresses) is reduced below the code-specified value it is generally possible to reduce the weight of the structure at the cost of increasing the response as long as the response is within the code limits. In this extension of our previous research, we generalize our computational model by minimizing the weight of the structure as well as the required level of control forces. This is done by adding another external layer to the formulation which includes constraints on the stresses, displacements, complex parts of the closed loop eigenvalues, and their corresponding closed loop damping factors. The last two sets of constraints are used to ensure reduction of the response to the allowable limits.

In the next section, we first present the formulation of the integrated structural/control optimization problem. Then, a new parallel-vector algorithm is presented for determination of the closed loop system sensitivities. Next, three example structures are presented, a one-span statically-indeterminate steel bridge structure, a continuous two-span statically-indeterminate steel bridge structure, and a steel multistorey space moment resisting frame. In a subsequent section, the memory and CPU time requirements for solution of the problem are discussed. The paper ends with conclusions.

2. INTEGRATED STRUCTURAL/CONTROL OPTIMIZATION

Linear actuators (providing forces in a linear direction) are distributed along the axis of a selected number of members in a frame structure (consisting of linear elements). Through the use of sensors measuring the response of the structure at various points and actuators, the response of the structure can be reduced. Broadly speaking, the control forces provide the opposite effects of externally applied dynamic forces. The problem is formulated by defining a control energy functional called control performance index (J) and minimizing it with respect to the state variables (displacements and velocities) and control forces satisfying the equations of motion. For details of the formulation of the open-loop (uncontrolled structure) and closed-loop (controlled structure) systems, see Adeli and Saleh (1997).

In order to minimize the weight of the controlled structure, constraints on stresses, displacements, closed-loop eigenvalues, and the corresponding damping factors are defined. In practical design of structures, members of the structure are divided into N_m groups and the same section is used for members of each group. Such a design linking strategy is employed in our formulation.

Minimize:

$$W(\mathbf{x}) = \sum_{m=1}^{M} \rho_m l_m x_m \tag{1}$$

subjected to

$$d_i^L \leqslant r_{ig}(\mathbf{x}) + u_i(\mathbf{x}, t) \leqslant d_i^U; \quad i = 1, 2, \ldots, I; \quad g = 1, 2, \ldots, G \tag{2}$$

$$\sigma_r^L \leqslant \sigma_{rg}(\mathbf{x}) + \sigma_r(\mathbf{x}, t) \leqslant \sigma_r^U; \quad r = 1, 2, \ldots, N_m \quad g = 1, 2, \ldots, G \tag{3}$$

$$x_m^L \leqslant x_m \leqslant x_m^U; \quad m = 1, 2, \ldots, M \tag{4}$$

$$\hat{\omega}_j \geqslant \bar{\omega}_j; \quad j = 1, 2, \ldots, J \tag{5}$$

$$\hat{\xi}_j \geqslant \bar{\xi}_j; \quad j = 1, 2, \ldots, J \tag{6}$$

where $W(\mathbf{x})$ is the objective function represented by the weight of the structure, $\mathbf{x}$ is the vector of design variables (cross sectional areas of the members of the structure), x_m, ρ_m,

and l_m are the cross-sectional area, mass density, and the total length of members belonging to the group m. The quantities $d_i^L, d_i^U, \sigma_r^L, \sigma_r^U, x_m^L$, and x_m^U are the lower and upper bounds on the nodal displacements, member stresses, and design variables, respectively. The quantities I, G, and J represent the number of constrained displacement degrees of freedom, static cases of loadings, and closed-loop eigenvalues, respectively. The quantities $\bar{\omega}_j$ and $\bar{\xi}_j$ represent lower bounds for the imaginary part of the jth closed-loop eigenvalue and its corresponding damping factor, respectively. The functions $r_{ig}(\mathbf{x})$ and $\sigma_{rg}(\mathbf{x})$ represent the displacement corresponding to the ith degree of freedom and the stress in the rth member due to the gth static loading case. The functions $u_i(\mathbf{x}, t)$ and $\sigma_r(\mathbf{x}, t)$ are the displacement corresponding to the ith degree of freedom and the stress in the rth member due to time-dependent dynamic loading.

Constraints are imposed on the imaginary part of the eigenvalues of the closed loop matrix, eqn (5), and the corresponding damping factor, eqn (6), so that the structure reaches the steady state in the least possible time, with minimum number of oscillations, and maximum damping. A non-zero imaginary part ensures a damping factor of less than one which is necessary for damped oscillation of the structure (a damping factor of one results in a non-oscillatory motion that will vanish over a longer period of time). Experience shows a lower bound on the damping factor, $\bar{\xi}_j$, in the range of 0.7 to 0.8 will minimize the deviation from the steady state response within the shortest time period. Similarly, for the lower bound on the imaginary part, $\bar{\omega}_j$, it was found that a value in the range of 0.75–1.0 times the real part of the smallest closed loop eigenvalue, $\hat{\sigma}_j$ (usually in the range of 1.0 to 2.0) will minimize the deviation from the steady-state response within the shortest time period.

The constrained optimization problem is transformed to an unconstrained optimization problem by defining a Lagrangian function to be solved by the optimality criteria approach. In this approach, sensitivities representing the changes in the constraints with respect to the design variables are needed for the solution. Computation of sensitivities for displacement, stress, closed-loop eigenvalues, and damping factors is given in Saleh and Adeli (1994b) and will not be repeated here. Recursive equations for redesign based on the sensitivity equations have also been developed, as presented in Saleh and Adeli (1994b).

3. PARALLEL-VECTOR ALGORITHM FOR THE CLOSED LOOP SYSTEM SENSITIVITIES

As an extension of our previous research, a parallel-vector algorithm has been developed for computation of the closed loop eigenvalue and damping factor sensitivities. The algorithm was implemented in C on a shared-memory vector supercomputer, Cray YMP8E/8128 using both multitasking and vectorization (Soegiarso and Adeli, 1994). Multitasking is done through a combination of microtasking and macrotasking (Saleh and Adeli, 1994a). The step-by-step details of the algorithm are given in Appendix II.

3.1. *Examples*

The computational model and parallel-vector algorithms have been applied to three example structures: a one-span steel bridge structure (Fig. 1), a two-span continuous steel bridge structure (Fig. 2), and a steel multistorey space moment resisting frame structure (Fig. 3).

3.1.1. *Example* 1 This example is a single-span steel truss bridge with a span of 48.6 m, height of 6 m, and width of 6 m (Fig. 1). The structure has 292 members and 76 nodes. This results in $(76-4)(6) = 432$ state variables (3 displacements and 3 velocities for each node of the structure). Four controllers are placed along the members in every vertical plane passing through the joints over the middle half of the span of the bridge as shown in Fig. 1 (10 panels). It is assumed that the bridge deck consists of a 17.78 cm (7 in) concrete deck. The bridge is initially designed for AASHTO live load of H20 (AASHTO, 1993) and according to the American Institute of Steel Construction (AISC) Allowable Stress Design (ASD) specifications (ASIC, 1989). Wide-flange shapes are selected for all the members of the bridge structure using A36 steel with yield stress of 248.2 MPa (36 ksi).

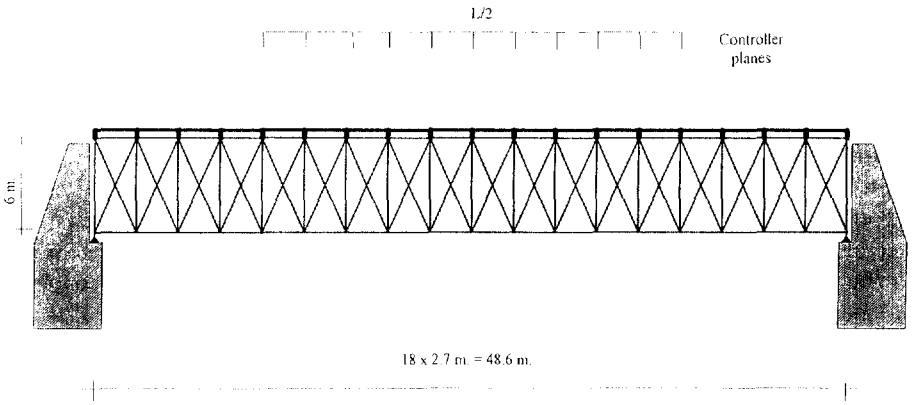

Fig. 1. Example 1. One-span truss bridge.

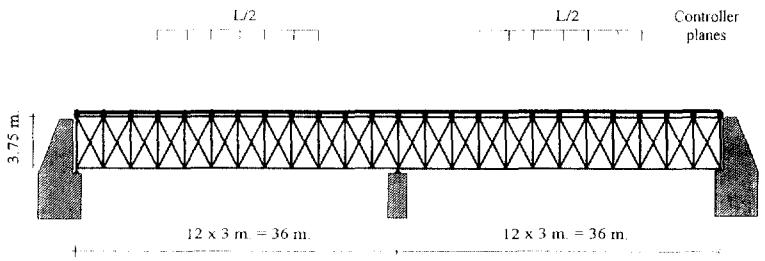

Fig. 2. Example 2. Two-span continuous truss bridge.

Then, three kinds of dynamic loadings are considered:

(a) A moving vertical impulse loading on each lane of the bridge moving in the same direction with a speed of 65 mph (105 km/h). The magnitude of this load is the resultant of the two axle loads of the AASHTO H20 loading. This load is multiplied by a δ function with a duration of 1 s.
(b) The 1940 El Centro earthquake ground acceleration record shown in Fig. 4 (Chopra, 1995).
(c) Periodic impulsive horizontal loadings (Fig. 5) on each joint of the truss (perpendicular to the plane of the truss) modeling the wind loading on the structure (pressure on one side and suction on the other side). The magnitude of the wind pressure is found using the AASHTO (1993) code and assuming a wind velocity of 160 kilometers per hour: $q = 3.59$ KN/m^2. Three other wind speeds of 80, 240, and 320 km/h are also used to study the effect of the wind speed on the minimum weight controlled structure.

The bridge structure is redesigned for one of the following load combinations satisfying all the AISC ASD stress requirements and AASHTO displacement requirement: $a+b$ or $a+c$. The member stresses are constrained to the allowable stresses specified by the AISC ASD code. The minimum weight of the uncontrolled structure with constraints on stresses and displacements is compared with minimum weight of the controlled structure with constraints on stresses, displacements, imaginary part of the closed loop eigenvalues and their corresponding damping factors. The maximum vertical displacement is constrained to $L/1000$ where L is the span length (AASHTO, 1993). The limits on the imaginary parts of the smallest two closed loop eigenvalues, $\bar{\omega}_j$, in eqn (5) are chosen 1.75 and the limit on the corresponding damping factors, $\bar{\xi}_j$ in eqn (6) is chosen as 0.7. This is based on the observation that for this structure, only the first two modes of vibration contribute to the response significantly (Adeli and Saleh, 1997).

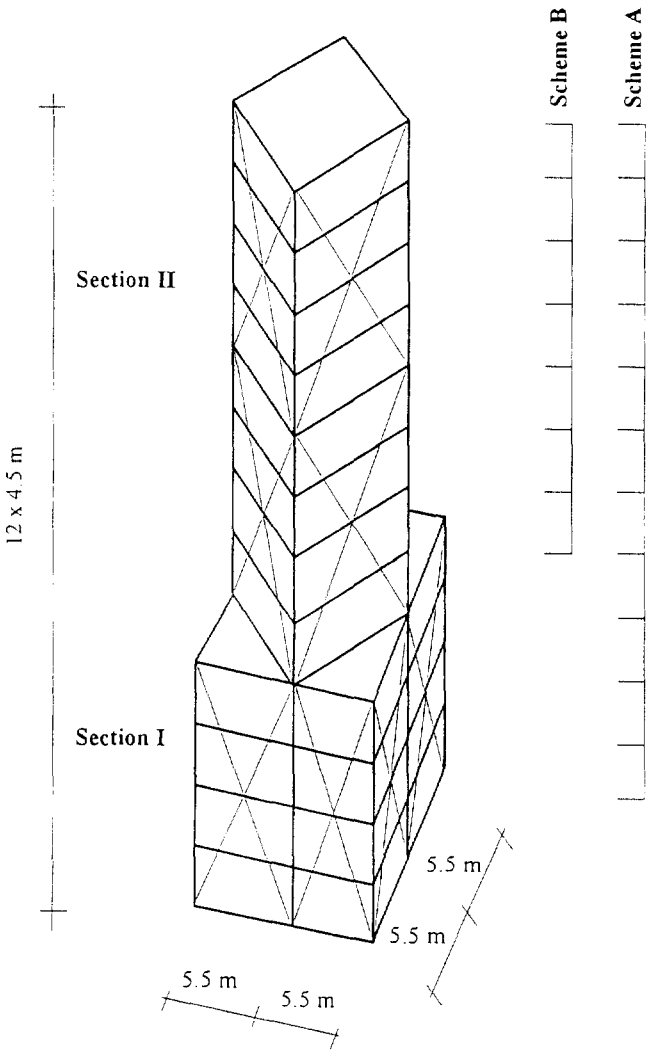

Fig. 3. Example 3. Twelve-story rotated-square structure. (a) Perspective view.

3.1.2. *Example* 2 This is a two-span continuous truss steel bridge with a total span length of 72 m, height of 6 m, and width of 6 m (Fig. 2). The structure has 388 members and 100 nodes. This results in $(100-6)(6) = 564$ state variables (3 displacements and 3 velocities for each node of the structure). In this example, four controllers are placed along the members in every vertical plane passing through the joints over the middle half of each span of the bridge as shown in Fig. 2 (6 panels). Loadings and constraints are the same as in Example 1.

3.1.3. *Example* 3 This example is a 12-story moment-resisting frame with a rotated-square plane and a height of 54 m, as shown in Fig. 3. The structure has 152 members and 68 nodes excluding supports. This results in 816 state variables (6 displacements and 6 velocities for each node of the structure). In this example, the controllers are placed in the horizontal plane of each floor diaphragm alongside beams in two perpendicular directions (principal axes of the floor plane when there are two axes of symmetry in the plan) using two different schemes, A and B. In scheme A, controllers are placed along the beams in every floor plane of the structure (12 in Section I and 4 in Section II). In scheme B, controllers are placed in every floor plane in Section II of the structure (8 floors). The actively controlled beams are identified with dashed lines in Fig. 3. The loading on the structure consists of uniformly distributed dead and live loads of 2.88 kPa (60 psf) and 2.38

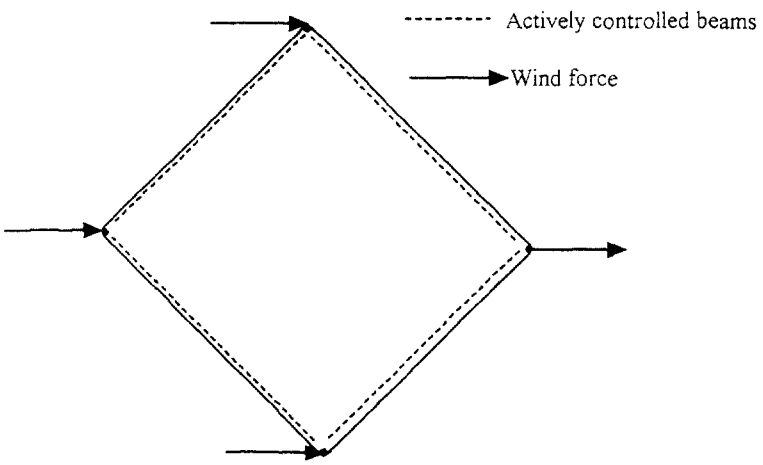

Plan for section II

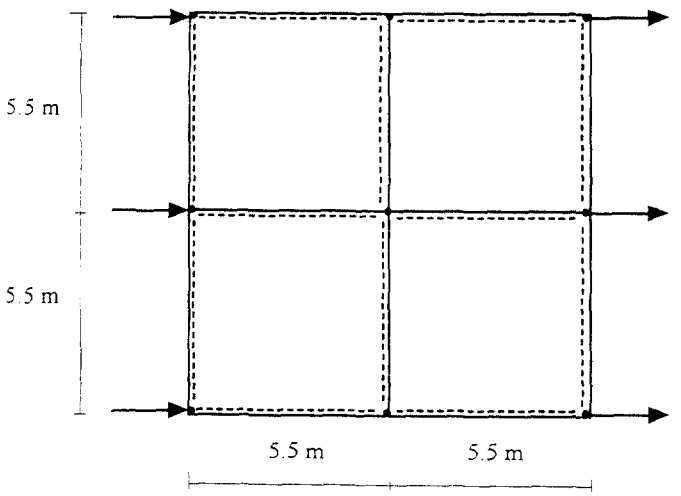

Plan for section I

Fig. 3(b). Plans and wind loading c.

kPa (50 psf) (office building), respectively. Wide-flange shapes from the AISC manual (AISC, 1989) are selected for all the members including bracings. In example 3a no bracing is used. In example 3b, cross bracings are used as identified in Fig. 3a to study the effect of bracings on the response and stresses of the controlled structure.

Three kinds of dynamic loadings are considered. Loadings *b* and *c* are used as in Example 1 except that for loading *c* the magnitude of the wind pressure is computed according to the Uniform Building Code (UBC, 1994) based on a basic wind speed of 113 km/h (70 mph), exposure C (generally open area), and an importance factor of 1. The forces are applied on each exterior joint of the frame (pressure on one side and suction on the other side) (Fig. 3b). Two other wind speeds of 208 and 320 km/h are also used to study the effect of the wind speed on the minimum weight controlled structure.

Another type of wind loading—*d*—is considered for this example. This loading is similar to *c* but wind forces on one half of the structure are applied in one direction (say, west–east direction) and on the opposite direction on the other half of the structure (say, east–west direction) (Fig. 3c) in order to simulate roughly the loading of a *twister*.

The multistorey structure is redesigned for one of the following load combinations satisfying all the AISC ASD stress and displacement requirements: *b*, *c*, or *d*. The minimum

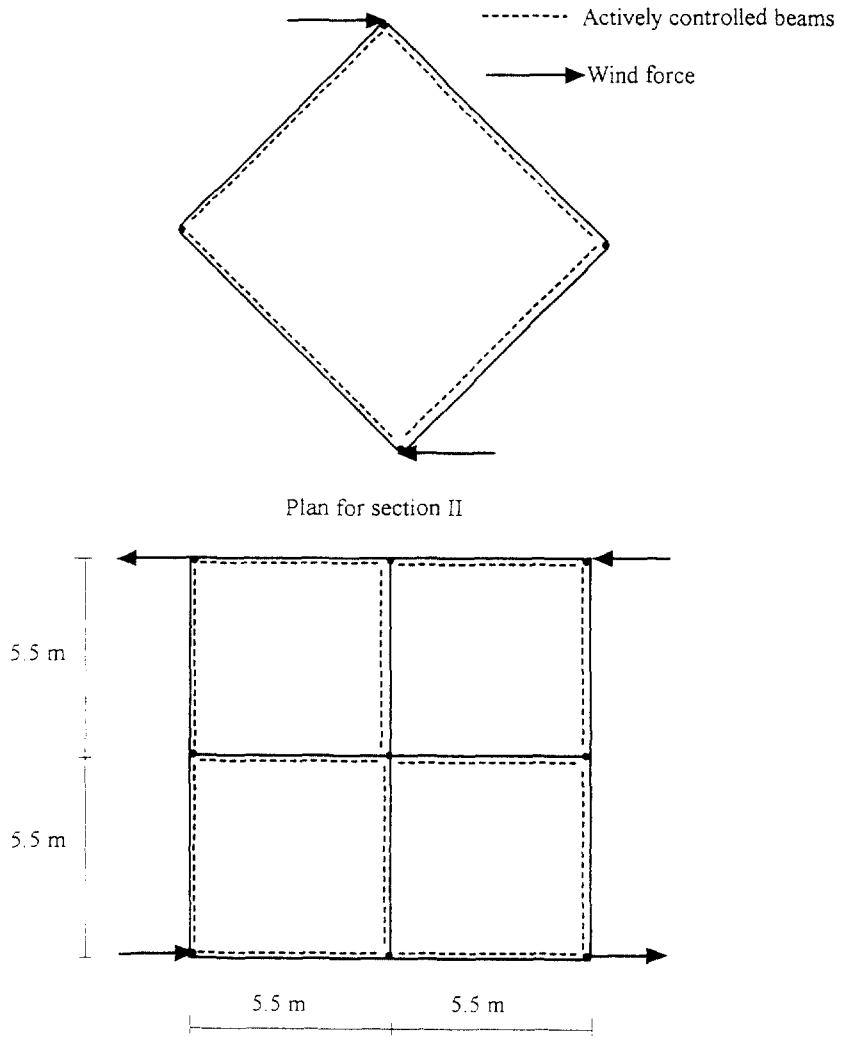

Fig. 3(c). Plans and wind loading d.

weight of the uncontrolled unbraced structure with constraints on stresses and displacements is compared with the minimum weight of the uncontrolled fully braced structure with constraints on stresses and displacements as well as the minimum weight of the controlled unbraced structure with constraints on the stresses, displacements, imaginary part of the closed loop eigenvalues and their corresponding damping factors. The interstorey drift is limited to 0.004 times the story height. The limit on the imaginary part of the two smallest closed loop eigenvalues, $\bar{\omega}_j$, in eqn (5) is chosen as 1.95 and the limit on the corresponding damping factors, $\bar{\xi}_j$ in eqn (6) is chosen as 0.725.

4. RESULTS

4.1. *Example* 1

Figure 6 shows the convergence histories for both uncontrolled and controlled structures subjected to combined impulsive traffic loading *a* and earthquake loading *b*. The minimum weight obtained for the controlled structure is 655 kN compared with minimum weight for the uncontrolled structure of 829 kN. Significantly, the minimum weight controlled structure is only 79% of the corresponding minimum weight for the uncontrolled

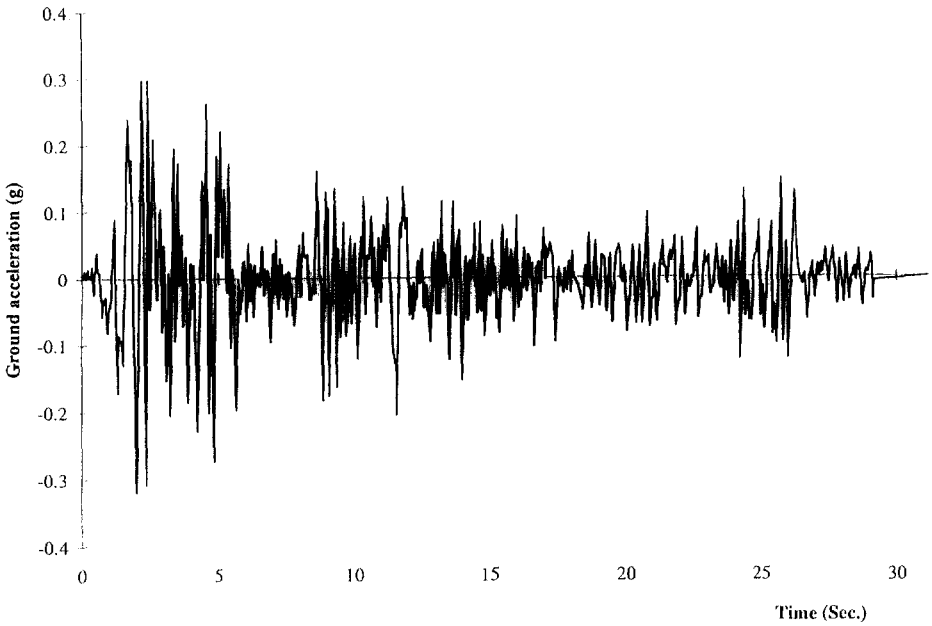

Fig. 4. The 1940 El-Centro (California) earthquake ground accelerations.

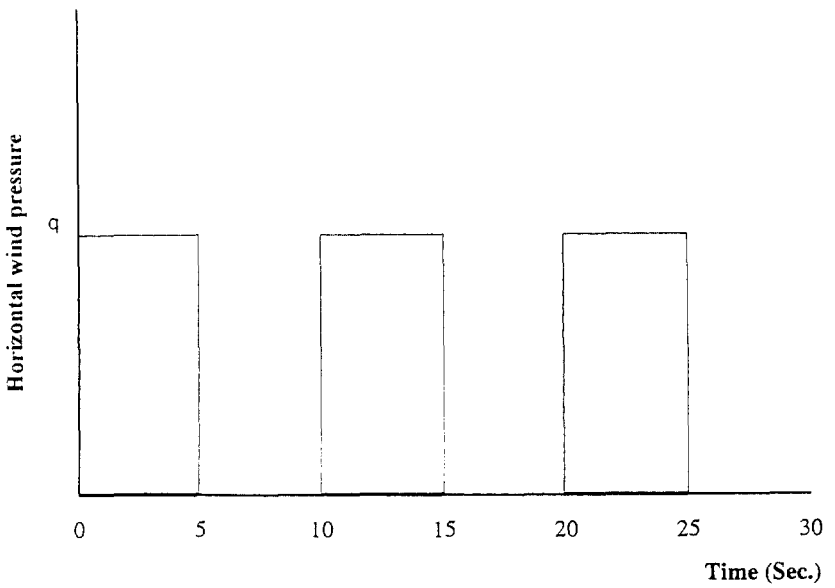

Fig. 5. Periodic impulsive horizontal wind pressure.

structure. The level of required control forces in this case is in the range 3.74 kN to 69.0 kN.

Figure 7 shows the convergence histories for both uncontrolled and controlled structures subjected to combined impulsive traffic loading *a* and wind loading *c*. The minimum weight obtained for the controlled structure is 596 kN compared with minimum weight for the uncontrolled structure of 716 kN. Significantly, the minimum weight controlled structure is only 83% of the corresponding minimum weight for the uncontrolled structure.

Figure 8 shows the variation of the weights of the minimum weight uncontrolled and controlled structures subjected to combined traffic loading *a* and wind loading *c* using four different wind velocities of 80 km/h, 160 km/h, 240 km/h, and 320 km/h.

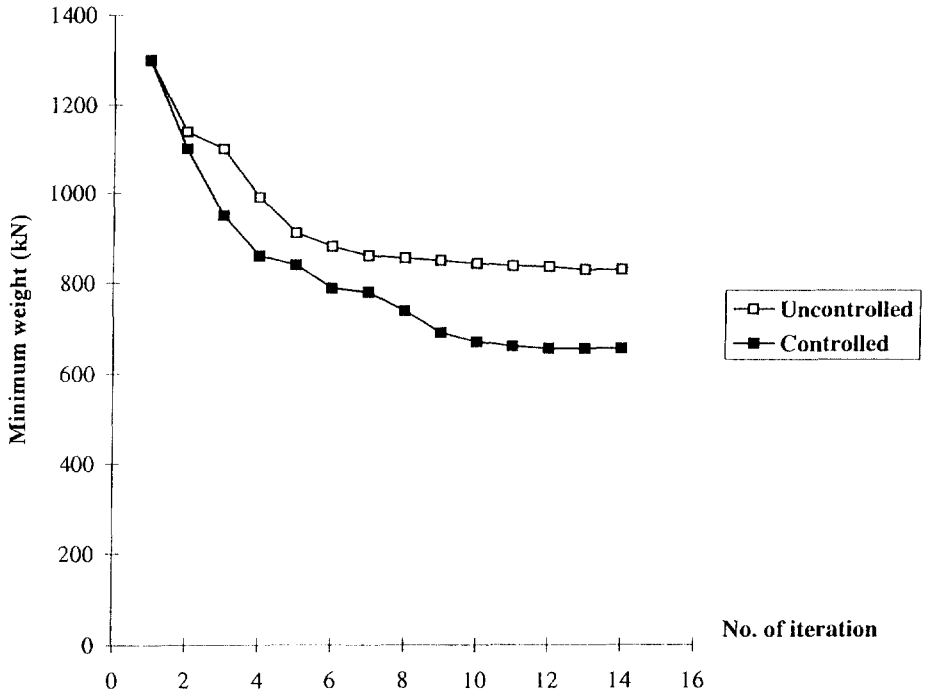

Fig. 6. Convergence histories for example 1 subjected to impulsive traffic and earthquake loadings.

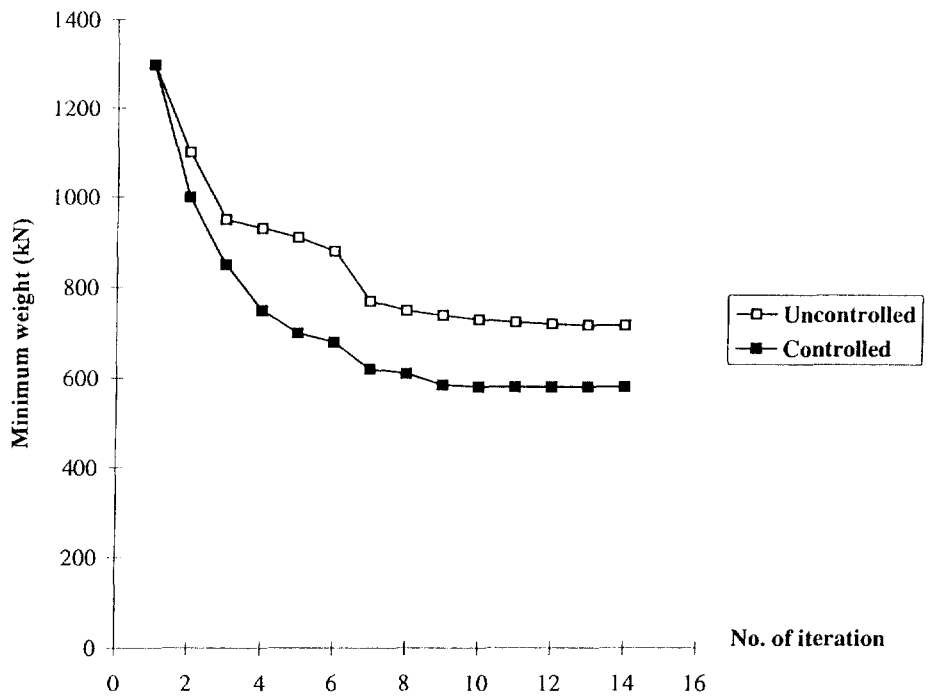

Fig. 7. Convergence histories for Example 1 subjected to impulsive traffic and wind loadings.

4.2. *Example* 2

Similar observations to those in Example 1 were made. It was also found that active controllers are more effective in reducing the weight of multispan continuous bridges than simply-supported single-span bridges.

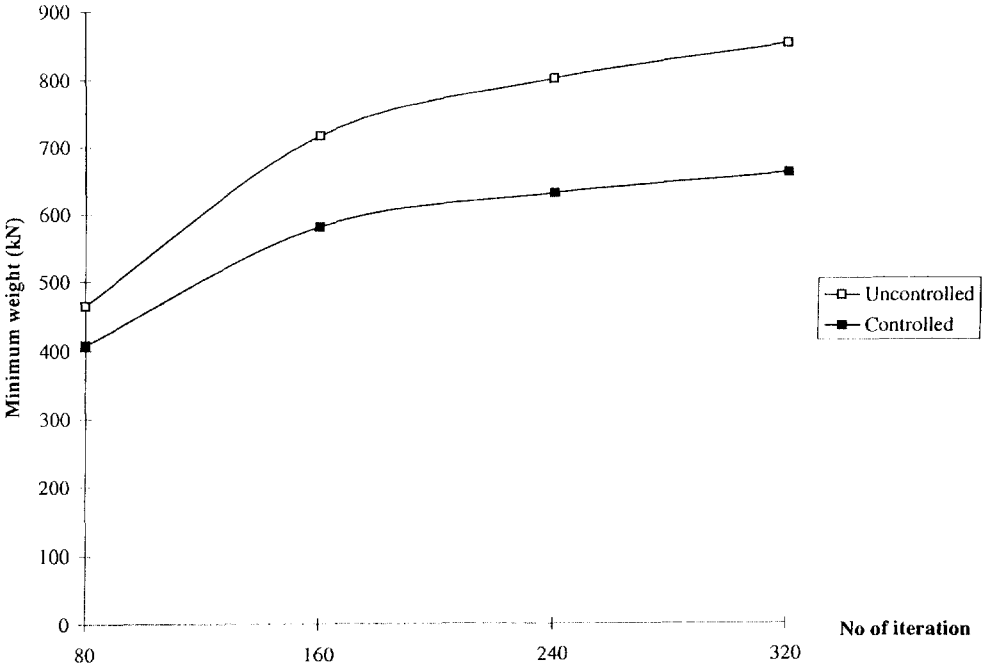

Fig. 8. Minimum weight uncontrolled and controlled structure for example 1 subjected to impulsive traffic and wind loadings using four different wind speeds.

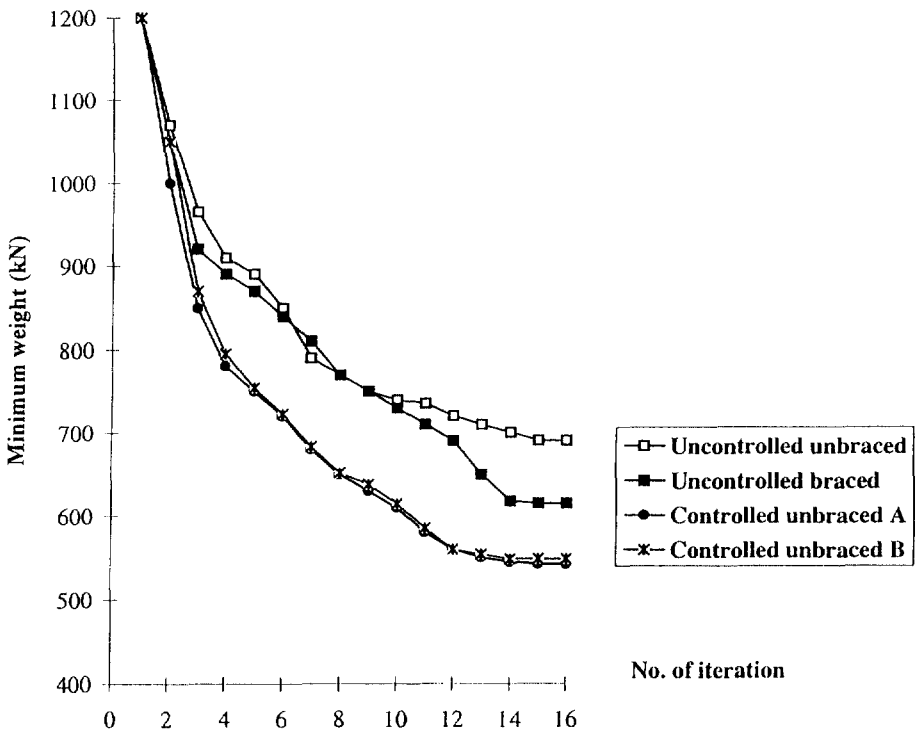

Fig. 9. Convergence histories for Example 3 subjected to impulsive traffic and earthquake loadings.

4.3. *Example* 3

Figure 9 shows the convergence histories for uncontrolled unbraced structure, uncontrolled braced structure, and controlled structure with two different schemes A and B for controllers subjected to earthquake loading *b*. The minimum weights obtained for the

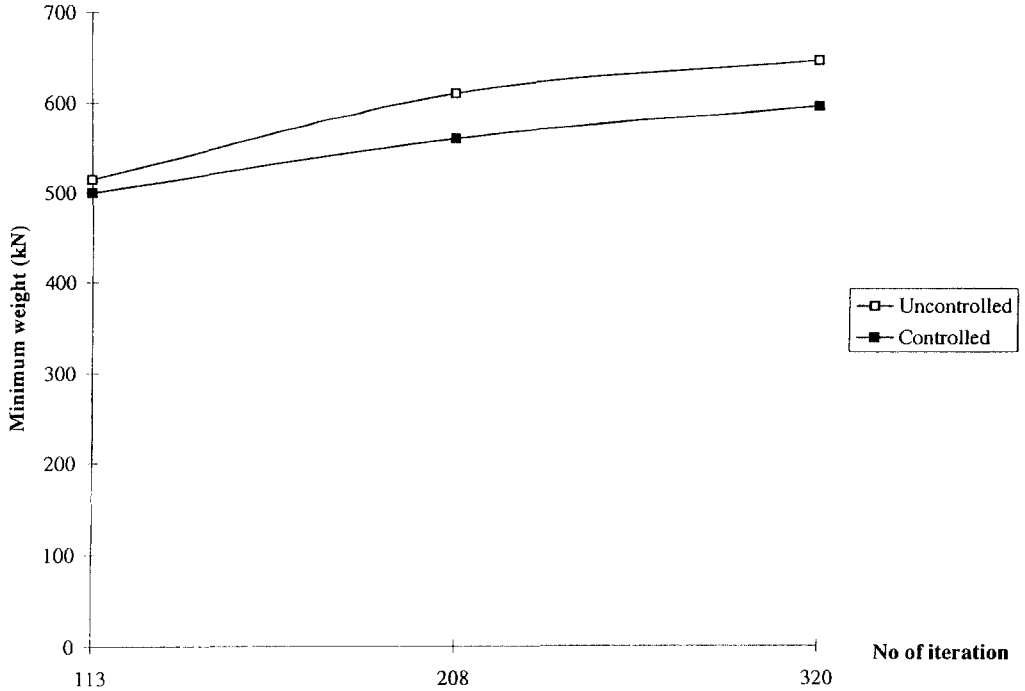

Fig. 10. Minimum weight uncontrolled and controlled structure for example 3 subjected to impulsive traffic and symmetric wind loadings using three different wind speeds.

uncontrolled unbraced and braced structures are 678 kN and 613 kN, respectively. The minimum weight controlled structure is 542 kN using controllers scheme A and 548 kN using controllers scheme B.

The level of required control forces for scheme A is in the range 8.64 kN to 144.0 kN and for scheme B is in the range 9.24 kN to 154.0 kN. The maximum forces are at the top of the structure. For scheme A, the level of control forces decreases gradually to 49% of the maximum force at the midheight of the structure and then decreases rapidly to 6% of the maximum force at the first floor. For scheme B, the level of control forces decreases to 37% of the maximum force at the midheight of the structure.

Figures 10 and 11 show variations of the weight of the minimum weight structure with the wind velocity for the case of symmetric wind loading *c* and unsymmetric (twister) wind loading *d*, respectively.

5. MEMORY AND CPU REQUIREMENTS

The solution of the integrated structural/control optimization problem for large-scale structures requires high-performance computing resources and large memory. It is important for the reader to have an appreciation of the size and complexity of the problem being solved.

The algorithms developed in this research have been implemented in C on the shared-memory supercomputer Cray YMP8E/8128 with 8 processors with a theoretical peak performance of 320 MFLOPS/processor (2.5 GFLOPS for 8 processors) and maximum shared memory (RAM) of 1024MB (128Mwords). However, the amount of RAM allocated to this research for processing time of more than 10 hrs was limited to 192MB. Mainframe computers can have a relatively large amount of memory. For example, the mainframe computer IBM 3090 can have a memory as large as 512MB. But, their processing power is only a fraction of supercomputers with vectorization and parallel processing capabilities.

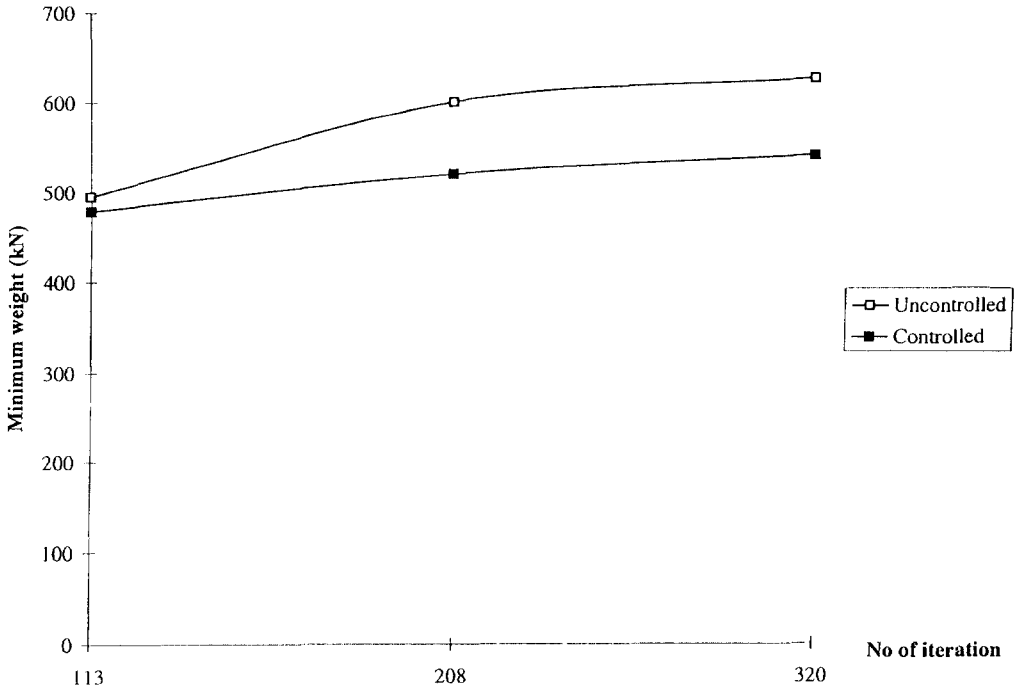

Fig. 11. Minimum weight uncontrolled and controlled structure for Example 3 subjected to impulsive traffic and unsymmetric (twister) wind loadings using three different wind speeds.

Hwang (1993) reports that one processor of Cray YMP8E/8128 without vectorization is 3.1 times faster than IBM 3090 and one processor of Cray C90, introduced in 1995, is 9.2 times faster than IBM 3090. Our experience with Cray supercomputers indicates that vectorization increases the speedup in the range of 10 (for complicated problems with large dependencies) to 20 (for simple problems). Thus, taking into account the vectorization capability, the Cray YMP8E/8128 is at least 30 times faster than IBM3090, even without using its parallel processing capability.

The largest example structure presented in this article (Example 3) has $N = 408$ displacement degrees of freedom and $2N = 816$ state variables. In each iteration, the solution of the resulting Riccati equation requires the solution of a complex eigenvalue problem for a matrix of size $4N \times 4N$ or 1632×1632. Subsequent to the solution of this eigenvalue problem, 816 sets of 816 complex linear equations must be solved. And this example needed 16 iterations to converge. Further, in each iteration, a complex eigenvalue problem of size 816×816 is solved four times (twice for the open loop system and twice for the closed loop system). The CPU time for one iteration of the integrated structural/control optimization problem using one processor of Cray YMP8E/8128 with vectorization was found to be 3 hrs and 21 min with vectorization performance of 207 MFLOPS. A rough estimate of the time required to solve the same example on the mainframe IBM 3090 would be 101 hrs per iteration and 67 days for the complete solution of the problem!

Now, we discuss the memory requirement. On the Cray YMP8E/8128, single and double precision real floating point variables require 8 and 16 bytes of memory, respectively. Single and double precision complex variables require 16 and 32 bytes of memory, respectively. All other data types require 8 bytes of memory per variable which is twice the corresponding number on mainframe computers. The maximum amount of memory used in the solution of Example 3 was found to be 168 MB. This includes the total memory needed for matrices representing the structural and control systems as well as the matrices used for temporary storage. For example, the real matrix of size $4N \times 4N$ or 1632×1632 for Example 3, formed for the solution of the Riccati equation, requires 21.3 MB of

memory. The resulting complex eigenvalues and corresponding complex eigenvectors of that matrix require 85.28 MB of memory. For the solution of each system of the 816 systems of 816 complex linear equations, 21.3 MB of memory is required.

The comparison of processing powers of mainframes and supercomputers with vectorization capability explains why high-performance multiprocessors are needed to solve the problem of integrated structural/control optimization for large structures. It has to be pointed out that we could have solved larger examples if more memory had been allocated for this research.

With the latest supercomputer technology, the present research can be applied to superhighrise building structures. For example, the latest Cray supercomputer, Cray C90 has 16 processors, maximum shared memory of 2.5 GB, and a peak theoretical processing speed of 16 GFLOPS. Using both vectorization and parallel processing, Cray C90 is roughly 14 times faster than the Cray YMP8E/8128.

6. CONCLUSIONS

A simultaneous integrated structural and control optimization approach has been formulated in this research employing actuator, control, and optimization technologies. Considering the numerically intensive and complex formulation of the problem, efficient parallel-vector algorithms were developed for solution of the problem utilizing the vectorization and multitasking capabilities of high-performance supercomputers. The computational model and algorithms were applied to two bridges and one building structure subjected to a variety of dynamic loadings.

The primary conclusion is that through adroit use of active controllers the weight of the minimum weight structure can be reduced substantially. The result would be a substantially lighter structure for both bridge and building structures. It was also found that active controllers are more effective in the case of severe dynamic loadings such as earthquake loading in reducing the weight of the minimum weight structure. They are also more effective in reducing the weight of multispan continuous bridges than simply-supported single-span bridges. In the case of impulsive wind loadings, the effectiveness of active controllers increases with an increase in the speed of wind, as demonstrated by Figs 8, 10 and 11.

For the multistorey building structure it was found that the controllers scheme B is almost as effective as scheme A. Thus, scheme B which requires a considerably fewer number of controllers is recommended.

With the rapid and continuous improvement of the actuator technology and increase in demand, their availability should increase and their price should decrease in coming years. Active controllers and the computational model and algorithms developed in this research give the future structural designers an effective means of reducing both the response of the structure and its weight. In some cases it may be desirable to reduce the response such as drift in highrise and superhighrise building structures to a minimum. In other cases achieving the lightest structure while keeping the response within the code-specified limits may be desirable.

The computational model and algorithms developed in this research are admittedly complex and advanced and even perhaps a bit futuristic. But, they provide the theoretical foundation for design and construction of a new generation of high-technology adaptive/smart structures. We have already demonstrated their practicality by applying them to rather realistic example structures. The future is already here!

Acknowledgements—Computing time for this research has been provided by the Ohio Supercomputing Center.

REFERENCES

AASHTO (1993) *Standard Specifications for Highway Bridges*, (15th Ed.). American Association of State Highway and Transportation Officials, Washington.

Adeli, H. (1992a) *Supercomputing in Engineering Analysis*. Marcel Dekker, New York, NY.

Adeli, H. (1992b) *Parallel Processing in Computational Mechanics*. Marcel Dekker, New York, NY.

Adeli, H. and Kamal, O. (1993) *Parallel Processing in Structural Engineering*. Elsevier Applied Science, London.
Adeli, H. and Saleh, A. (1997) Optimal Control of Adaptive/Smart Bridge Structures. *Journal of Structural Engineering, ASCE* **123,** (Suppl. 2), 218–226.
AISC (1989) *Manual of Steel Construction-Allowable Stress Design* (8th ed.). American Institute of Steel Construction, Chicago.
Chopra, A. K. (1995) *Dynamics of Structures: Theory and Applications to Earthquake Engineering*. Prentice Hall, Englewood Cliffs, NJ.
Housner, G. W., Soong, T. T. and Marsi, S. F. (1996) Second Generation of the Active Structural Control in Civil Engineering. *Microcomputers in Civil Engineering* **11,** (Suppl. 5).
Hwang, K. (1993) *Advanced Computer Architecture Parallelism, Scalability, Programmability*. McGraw Hill, New York.
Kobori, T. (1996) Future Directions on Research and Development of Seismic-Response-Controlled Structures. *Microcomputers in Civil Engineering* **11,** (Suppl. 5).
Liu, S. C., Eeri, M., Lagorio, H. J. and Chong, K. P. (1991) Status of U.S. Research on Structural Control Systems. *Earthquake Spectra* **7**(4), 543–550.
Meirovich, L. (1990) *Dynamics and control of Structures*, John Wiley & Sons, NY.
Saleh, A. and Adeli, H. (1994a) Microtasking, Macrotasking, and Autotasking for Structural Optimization. *Journal of Aerospace Engineering, ASCE* **7**(2), 156–174.
Saleh, A. and Adeli, H. (1994b) Parallel Algorithms for Integrated Structural/Control Optimization. *Journal of Aerospace Engineering, ASCE* **7**(3), 297–314.
Saleh, A. and Adeli, H. (1996) *Parallel Eigenvalue Algorithms for Large Scale Control-Optimization Problems. Journal of Aerospace Engineering, ASCE* **9**(3), 70–79.
Saleh, A. and Adeli, H. (1997) Robust Parallel Algorithms for Solution of the Riccati Equation. *Journal of Aerospace Engineering, ASCE* **10**(3).
Soegiarso, R. and Adeli, H. (1994) Impact of Vectorization on Large-Scale Structural Optimization. *Structural Optimization* **7**(1,2), 117–125.
UBC (1994) *Uniform Building Code*, Vol. 2-*Structural Engineering Design Provisions*, International Conference of Building Officials, Whitter, CA.

APPENDIX 1: NOTATIONS

$\mathbf{A}$ = plant matrix
$\bar{\mathbf{A}}$ = the closed-loop matrix
$\mathbf{B}$ = input matrix
$d_i^{\mathrm{L}}, d_i^{\mathrm{U}}$ = the lower and upper bounds on the nodal displacements
$\mathbf{e}$ = right eigenvector matrix
$\mathbf{e}'$ = left eigenvector matrix
G = number of static cases of loadings
I = number of constrained displacements
J = number of closed-loop eigenvalues
$\mathbf{K}$ = structure stiffness matrix
$\mathbf{K}_{\mathrm{m}}$ = member stiffness matrix
l_{m} = total length of the members belonging to group m
M = number of design variables
$\mathbf{M}$ = structure mass matrix
$\mathbf{M}_{\mathrm{m}}$ = member mass matrix
N = number of degrees of freedom
N_{f} = number of actuators
N_{m} = total number of the members belonging to group m
n_{p} = number of processors
$\mathbf{P}$ = Riccati matrix
q = wind pressure
$\mathbf{R}$ = control weighting matrix

$r_{ig}(\mathbf{x})$ = displacement at the ith degree of freedom due to the gth loading case
$W(\mathbf{x})$ = weight of the structure
$\mathbf{u}_i(\mathbf{x}, t)$ = displacement of the ith degree of freedom due to dynamic loading
$\mathbf{x}$ = vector of design variables
$\mathbf{x}_m$ = cross-sectional area of the members belonging to group m
$x_m^{\mathrm{L}}, x_m^{\mathrm{U}}$ = lower and upper bounds on the design variables
ρ_m = mass density of the members belonging to group m
$\sigma_r^{\mathrm{L}}, \sigma_r^{\mathrm{U}}$ = lower and upper bounds on the member stresses
$\sigma_r(\mathbf{x}, t)$ = stress in the rth member due to dynamic loading
$\sigma_{rg}(\mathbf{x})$ = stress in the rth member due to the gth static loading case
ω_j = imaginary part of the jth eigenvalue of the unsymmetric closed-loop matrix
$\bar{\omega}_j$ = lower bound on the imaginary part of the jth eigenvalue
ξ_j = jth damping factor of the unsymmetric closed-loop matrix
$\bar{\xi}_j$ = lower bound on the jth damping factor of the unsymmetric closed-loop matrix

APPENDIX II: PARALLEL-VECTOR ALGORITHM FOR THE CLOSED LOOP SYSTEM SENSITIVITIES

Input: N, $N_m N_r$, n_p, δT, T, $\mathbf{A}$, $\bar{\mathbf{A}}$, $\mathbf{B}$, $\mathbf{e}$, and $\mathbf{e}'$.

FOR $p = 1$ UNTIL n_pDO (Macrotasking)

$m = p$

Calculate $\mathbf{K}_m$, M_m
NEXT p
FOR $p = 1$ UNTIL n_pDO (Microtasking)

$m = p$

(a) FOR $j = 1$ UNTIL N DO

$$\omega_{j,m}^2 = \frac{1}{X_m} \boldsymbol{\Phi}_{jm}^T (\mathbf{K}_m - \omega_j^2 \mathbf{M}_m) \boldsymbol{\Phi}_{j,m} \quad \text{(Vectorization)}$$

$$\boldsymbol{\Phi}_{j,m} = \sum_{i=1}^{N} \frac{1}{X_m(\omega_i^2 - \omega_j^2)} \boldsymbol{\Phi}_{j,m}^T (K_m - \omega_i^2 \mathbf{M}_m) \boldsymbol{\Phi}_{i,m} \boldsymbol{\Phi}_i : \quad \text{(Vectorization)}$$

NEXT j

$$\mathbf{A}_m = \begin{bmatrix} 0 & 0 \\ -\omega_{i,m}^2 & 2\xi\omega_{i,m} \end{bmatrix} \quad i = 1, 2, \ldots, N \quad \text{(Vectorization)}$$

$$\mathbf{B}_m = \begin{bmatrix} 0 \\ \boldsymbol{\Phi}_{i,m}^T \mathbf{D}_0 \end{bmatrix} \quad i = 1, 2, \ldots, N \quad \text{(Vectorization)}$$

FOR $i = 1$ UNTIL 2N DO
FOR $j = 1$ UNTIL 2N DO

$$(\mathbf{Z}_m)_{ij} = \sum_{k=1}^{N} (\mathbf{B}_m)_{ik} * (\mathbf{R}^{-1})_{ik} * \mathbf{B}_{kj}^T + \mathbf{B}_{ik} (\mathbf{R}^{-1})_{kk} * (\mathbf{B}_m^T)_{kj} \quad \text{(Vectorization)}$$

NEXT j
NEXT i
FOR $i = 1$ UNTIL $2N$ DO
FOR $j = 1$ UNTIL $2N$ DO

$$\mathbf{H}_{ij} = \sum_{k=1}^{2N} (\mathbf{A}_m^T)_{ij} * \mathbf{P}_{kj} - \mathbf{P}_{ik} * (\mathbf{A}_m^T)_{kj} + (\mathbf{P} * \mathbf{Z}_m)_{ik} * \mathbf{P}_{kj} \quad \text{(Vectorization)}$$

NEXT j
NEXT i
FOR $i = 1$ UNTIL $2N$ DO
FOR $j = 1$ UNTIL $2N$ DO

$$\mathbf{S}_{ij} = \sum_{k=1}^{2N} \mathbf{e}_{ik}^T * \mathbf{H}_{kj} \quad \text{(Vectorization)}$$

$$\mathbf{S}_{ij} = \left(\mathbf{S}_{ij} + \sum_{k=1}^{2N} \mathbf{S}_{ik} * \mathbf{e}_{kj} \right) / (\hat{\lambda}_i + \hat{\lambda}_j) \quad \text{(Vectorization)}$$

NEXT j
NEXT i
FOR $i = 1$ UNTIL $2N$ DO
FOR $j = 1$ UNTIL $2N$ DO

$$(P_m)_{ij} = \sum_{k=1}^{2N} \mathbf{S}_{ik} * \mathbf{e}_{kj}'^T \quad \text{(Vectorization)}$$

NEXT j
NEXT i
FOR $i = 1$ UNTIL $2N$ DO
FOR $j = 1$ UNTIL $2N$ DO

$$(\bar{\mathbf{A}}_{,\mathrm{m}})_{ij} = (\mathbf{A}_{,\mathrm{m}})_{ij} - \sum_{k=1}^{2N} (\mathbf{Z}_{,\mathrm{m}})_{ij} * \mathbf{P}_{kj} - \sum_{k=1}^{2N} \mathbf{Z}_{ik} * (\mathbf{P}_{,\mathrm{m}})_{kj} \quad \text{(Vectorization)}$$

NEXT j
NEXT i
FOR $i = 1$ UNTIL $2N$ DO
FOR $j = 1$ UNTIL $2N$ DO

$$s_j = \sum_{k=1}^{2N} (\mathbf{e}_i^{'T})_k * (\bar{\mathbf{A}}_{,\mathrm{m}})_{kj} \quad \text{(Vectorization)}$$

NEXT j
NEXT i
FOR $i = 1$ UNTIL 2N DO

$$\hat{\lambda}_{i,\mathrm{m}} = \sum_{k=1}^{2N} s_k * \mathbf{e}_k \quad \text{(Vectorization)}$$

$\hat{\omega}_{i,\mathrm{m}} = \text{imaginary}(\hat{\lambda}_{i,\mathrm{m}})$
$\hat{\sigma}_{i,\mathrm{m}} = \text{real}(\hat{\lambda}_{i,\mathrm{m}})$

NEXT i
FOR $i = 1$ UNTIL $2N$ DO (Vectorization)

$$\xi_{i,\mathrm{m}} = \frac{(\hat{\omega}_i \hat{\sigma}_j \hat{\omega}_{i,m} - \hat{\omega}_i^2 \hat{\sigma}_{i,m})}{(\hat{\omega}_i^2 + \hat{\sigma}_i^2)^{3/2}}$$

NEXT i

$m = m + n_{\mathrm{p}}$

IF $m \leqslant \mathrm{N_m}$ THEN Go to (a)
NEXT p
STOP